JOURNAL OF CATALYSIS 144, 202–213 (1993)

The Effect of Loading of Vanadia on Silica in the Oxidation of Butane

L. OWENS AND H. H. KUNG[1]

Ipatieff Laboratory and Department of Chemical Engineering, Northwestern University, Evanston, Illinois 60208-3120

Received February 18, 1993; revised June 14, 1993

The effect of vanadium loading on the structure and the catalytic behavior of silica-supported vanadium oxide catalysts in the selective oxidation of butane was investigated in a continuous flow reaction system using catalysts containing loadings of 0.53, 0.58, or 6.4 wt% vanadium supported on Davison or Cabosil silica. The lower loading samples were found to be more selective for oxidative dehydrogenation. At 520°C, with a feed of $He/O_2/C_4H_{10}$ = 88/8/4 at a total flow rate of 100 ml/min, the total dehydrogenation selectivity on the 0.58 wt% V sample was 65 and 50% at butane conversions of 5 and 20%, respectively, whereas they were 42 and 5% on the 6.4 wt% V samples. The activation energies for the oxidation of butane were about 110 kJ/mol for the lower loading samples and 164 kJ/mol for the higher loading samples. At 520°C, the activity per vanadium was comparable for the different samples. Laser Raman spectra of fresh catalysts indicated that only a well-dispersed vanadia species existed on the 0.58 wt% V sample, while crystalline V_2O_5 was also formed on the 6.4 wt% V samples. The ratio of well-dispersed to crystalline vanadia species on the fresh catalysts was higher for the Cabosil silica-supported sample than the Davison silica-supported sample. After reaction, the spectra of the 0.58 wt% V samples did not indicate any changes. However, significantly more crystalline V_2O_5 was found on the 6.4 wt% V samples on both silica supports, indicating that aggregation of vanadia had occurred during reaction. The higher total dehydrogenation selectivity on the 0.58 wt% V samples was attributed to the presence of the well-dispersed vanadia, while the presence of crystalline V_2O_5 species on the higher loading samples contributed to the production of total oxidation products.

INTRODUCTION

Catalysts based on vanadium oxide are frequently used in selective oxidation reactions due to their high activity and selectivity for partial oxidation products. Over the years, it has been found that the catalytic properties of V_2O_5 can be enhanced by oxide supports such as alumina and, especially, titania (*1, 2*). It is accepted that the vanadia species interact with the support in various forms depending on the nature of the support such that VO_x units on the supports can be quite different from those in V_2O_5 (*3–5*). In general, at low loadings, vanadia exists in a highly dispersed form. Crystallites of V_2O_5 form only at high loadings. The interaction of vanadia with silica and the structure of the VO_x units on the support have been studied by a number of investigators recently (*6–17*). While differences existed in the details in these reports due to the type of silica used and its physical properties, it has been observed that in general, highly dispersed monomeric surface vanadia species proposed to be $(Si–O)_3{\equiv}V{=}O$ and possess a characteristic peak at about 1040 cm^{-1} in the laser Raman spectrum were found on silica-supported samples with very low loadings of vanadia (*13–15, 18*). Crystalline V_2O_5 has been detected on the samples well below an equivalent of monolayer coverage as the vanadium loading was increased. On other supports such as alumina, dispersed surface polyvanadate species characterized by laser Ra-

[1] To whom correspondence should be addressed.

0021-9517/93 $5.00

man peaks at 860–960 cm^{-1} have also been reported to exist (*17, 19*). These polyvanadate species have not been detected on silica.

There have been several studies on alkane oxidation using silica-supported vanadia catalysts (*20–24*). However, only a few have investigated the effects of loading and structure. Oyama and Somorjai (*23*) studied the oxidation of ethane over Cabosil silica-supported vanadia and proposed that at ethane conversions of less than 2%, the reaction of ethane to selective oxidation products ethene and ethanal was structure-insensitive while the reaction to CO_x was structure-sensitive. In contrast, Le Bars *et al.* (*24*) also studied the oxidation of ethane over silica-supported vanadia and found that the rate of production of ethene (in mol/s-g V_2O_5) reached a maximum at less than 1 wt% vanadia loading, and decreased as the loading was increased to 20 wt% V_2O_5. Thus, there are indications that the catalytic behavior of these different vanadia species on silica for alkane oxidation varies. We report here our investigation of the effect of loading on the structure and catalytic behavior of silica-supported vanadia catalysts for the oxidation of butane.

EXPERIMENTAL

Catalyst Preparation

Davison silica Grade 62 (250 m^2/g) and amorphous fumed Cabosil silica Grade EH-5 (380 m^2/g) were used as support. The Davison silica was washed to remove sodium and calcium impurities by stirring in 1.0 *M* nitric acid at 85–90°C for 3–4 days, washing in deionized water by decantation, drying at 100°C overnight, and heating to 550°C for 5–6 hours. This silica was labelled AWS. The AWS-supported samples were prepared using impregnation by incipient wetness with aqueous solutions of ammonium metavanadate (Johnson Matthey 99.99%) with 2 mol of oxalic acid (Alfa 99%) added for every mole of ammonium metavanadate used. Approximately 1 ml of deionized water per gram of silica was used to prepare the solutions. The samples were dried overnight at 100°C and calcined at 550°C for 6 h. The surface areas of the 6.4V-AWS and 0.58V-AWS were measured using N_2 adsorption to be 150 and 230 m^2/g, respectively.

The Cabosil silica was used as received. The supported vanadia samples were prepared as the AWS samples using impregnation by incipient wetness. They were dried at 300°C for 2 h before calcination at 550°C for 6 h.

The concentrations of impurities and vanadium in the samples were determined using inductively coupled plasma (ICP). To prepare for ICP analysis, the samples were dissolved in 100 ml of a 0.1 vol% HF solution. The catalysts prepared with the AWS were found to contain 6.4 wt% V and 0.58 wt% V. These samples are labelled 6.4V-AWS and 0.58V-AWS, respectively. Similarly, Cabosil silica-supported samples containing 6.4 wt% V and 0.53 wt% V are labelled 6.4V-Cab and 0.53V-Cab, respectively.

Unsupported V_2O_5 was prepared by calcining ammonium metavanadate (99.99%) at 550°C for 6 h. The surface area of the unsupported V_2O_5 was measured using N_2 adsorption to be approximately 3 m^2/g.

Reaction Studies

Reactions were conducted in a quartz microreactor of 13 mm i.d. at 500, 520, or 540°C and near atmospheric pressure. The total flow rate was 50, 100, or 200 ml/min with a feed composition of $He/O_2/C_4H_{10}$ = 88/8/4. Between 0.015 and 1.5 g of the catalyst was packed between quartz wool plugs. Quartz chips were used to dilute the 6.4V-AWS and 6.4V-Cab samples to a bed length of approximately 1 cm. The remaining reactor volume was filled with quartz chips to quench gas-phase reactions. When an empty reactor was filled with quartz chips, the butane conversion was negligible at 520°C. A thermocouple inside the catalyst bed was used to record the reaction temper-

ature. Product gases were analyzed with on line gas chromatography. A 6-ft molecular sieve column operated at room temperature was used to detect CO and O_2, and a 20-ft VZ-7 column (Alltech) at room temperature was used to detect CO_2 and hydrocarbons. An 8-ft Graphpac GB column (Alltech) temperature programmed from 120 to 190°C was used to screen for oxygenates. The products detected were CO, CO_2, ethene/ethane, propane/propene, 1-butene, *cis*-, and *trans*-2-butene, 1,3-butadiene, and small quantities of oxygenates including ethanal, propanal, and maleic anhydride. Conversions were defined as the percentage of butane in the feed which has reacted. Selectivities were defined as the percentage of butane reacted to a specific product. The carbon balances in all the experiments were within 100 ± 4%. At low conversions, the conversion varied linearly with the W/F ratio (W is catalyst weight, F is feed flow rate). Thus the kinetics was not affected by external mass transfer effects. Furthermore, catalysts prepared with mesh sizes from 60 to 200 showed no variation in catalytic activity or selectivity. Thus pore diffusion was not limiting either.

Laser Raman Spectroscopy

Laser Raman spectra were collected using the 514.5-nm line of a Coherent INOVA 70-2 Ar ion laser. A laser power of 25 mW was used and the spectra were collected for 150 to 1000 s. Approximately 0.2 g of each sample was pressed into a pellet. Fresh 6.4V-AWS and 6.4V-Cab samples were pretreated by heating *in vacuo* at 520°C for 1 h to remove adsorbed water and then were exposed to 1 atm dry O_2 at 520°C for 0.5 h. The spectra were collected in O_2. Fresh 0.58V-AWS and 0.53V-Cab samples were treated as described above at 600°C.

To obtain spectra of the 6.4V-AWS, 6.4V-Cab and 0.58V-AWS samples that had been used for reaction, the reactor was purged with He at reaction temperature immediately after the reaction run. The sample was then treated in a flow of 63 ml/min of a He/O_2 (13 vol% O_2) mixture at 520°C for 3 h. The sample was cooled in this He/O_2 stream, and without exposure to air, pressed into a wafer and transferred to the sample holder in a dry box with an N_2 atmosphere. Raman spectra were collected without further treatment. The 0.53V-Cab sample was exposed to air after reaction, then heated in vacuo at 600°C for 1.0 h, and then exposed to 1 atm dry O_2 at 600°C for 0.5 h before the spectra were collected in O_2.

Thermogravimetric Analysis

Thermogravimetric analysis (TGA) were conducted with a TC2 Dupont 9900 instrument. A sample each of 0.58V-AWS and 6.4V-AWS, sufficient to produce approximately 20% butane conversion, were exposed to the reaction conditions as described above for 4 h. The samples were then transferred to the TGA cell. A stream of He with 10 vol% O_2 at 80 ml/min was passed over the sample while the temperature was raised at 10°C/min to 100°C to remove adsorbed water. The temperature was held at 100°C for 60 min and then raised at 10°C/min to 600°C.

The carbonaceous residues formed on the 0.58V-AWS and 6.4V-AWS samples were analyzed by measuring the amount of CO_2 burned off from samples that had been used for reaction for 2 h. The amounts of catalysts used were sufficient to effect about 20% butane conversion. After reaction, the reactor was purged with He for 1 h at reaction temperature. The samples were then heated at 520°C in a flow of He and 6.4 vol% O_2 for 10–15 min. Approximately 0.2 g of a 1.5 wt% Pt/SiO_2 catalyst was placed in series after the vanadia catalyst to combust any CO or other desorbed organic products to CO_2. A trap filled with Chromosorb P packing kept at approximately −95°C with an acetone slush bath was used to trap the CO_2 for gas chromatographic analysis later.

RESULTS

Reaction Studies

The predominant products in the oxidation of butane over the four catalysts studied

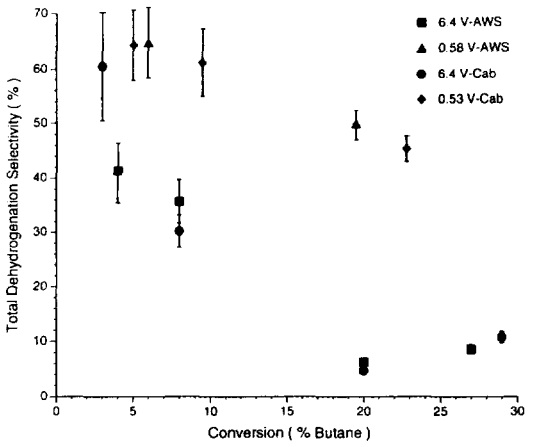

FIG. 1. Total dehydrogenation selectivity (1-butene, *cis*- and *trans*-2-butene, and 1,3-butadiene) versus butane conversion at 520°C, $He/O_2/C_4H_{10}$ = 88/8/4, 1 atm.

were dehydrogenation products (1-butene, *cis*- and *trans*-2-butene and 1,3-butadiene) and combustion products (carbon oxides). Small amounts of lower hydrocarbons and oxygenates were also detected. Figure 1 shows the dependence of selectivity for oxidative dehydrogenation products (butenes and butadiene) on butane conversion. Over the range of conversions studied, the selectivity was found to be higher on the 0.58V-AWS and 0.53V-Cab samples than the 6.4V-AWS and 6.4V-Cab samples. No dehydrogenation products were detected with unsupported V_2O_5 at these conversions. Table 1 shows a more detailed listing of some representative product distributions for these samples. As indicated in Table 1, at the reaction conditions investigated, the unsupported silica was slightly active. However, the yield of dehydrogenation products produced on the silica was too small to account for the differences in dehydrogenation selectivity between the vanadia samples.

Before reaction, the 6.4V-AWS and 6.4V-Cab samples were dark orange. However, after reaction these samples turned dark green or black. The original orange color of both samples was restored only after treatment at elevated temperatures in a flow of He and O_2. The 0.58V-AWS and 0.53V-Cab samples were light yellow before reaction. They were white immediately after reaction, but returned to their original light-yellow color once exposed to air.

Activation energies for the samples were determined over the temperature range 500 to 540°C using conversion data from 0 to 5%. They were found to be 112 ± 15 and

TABLE 1

Reaction Data for V/SiO_2 at 520°C, $He/O_2/C_4H_{10}$ = 88/8/4

Catalyst	wt(g)	Flow rate cm^3/min	Conv(%)	Selectivity (%)									Dehy. yield[c]
				CO	CO_2	C_2/C_3	1-C_4	*t*-C_4	*c*-C_4	1,3-C_4	Oxy.[a]	TDS[b]	
6.4V-Cab	0.0159	200	3.0	15	17	8	26	20	14	0	0	60	1.8
6.4V-Cab	0.026	100	8.0	39	26	5	14	7	6	3	5	30	2.4
6.4V-Cab	0.1	100	20.0	56	27	0	5	3	2	1	6	11	2.2
6.4V-Cab	0.15	100	29.0	56	34	0	2	1	1	0	5	4	1.2
6.4V-AWS	0.0249	200	4.0	28	23	8	21	11	9	0	0	41	1.6
6.4V-AWS	0.15	200	20.0	56	31	1	6	3	3	0	0	12	2.4
0.53V-Cab	0.2	100	5.0	8	14	10	22	19	17	6	4	64	3.2
0.53V-Cab	0.5	50	22.8	19	11	11	23	7	9	7	14	46	10.4
0.58V-AWS	0.2	100	6.0	12	10	6	26	15	15	9	7	65	3.9
0.58V-AWS	0.5	100	20.0	15	15	9	22	10	10	8	10	50	10.0
V_2O_5[d]	1.5	50	11.0	34	58	0	7	0	0	0	0	7	0.8
AWS	1.5	100	4.0	34	13	19	9	10	8	8	0	35	0.93/g cat
Cabosil	0.25	100	1.5	3	14	16	31	18	16	0	0	65	3.91/g cat

[a] Possible oxygenates include acetaldehyde, acetone, and propionaldehyde.
[b] TDS = total dehydrogenation selectivity.
[c] Dehy. yield = (% conv) × (selectivity), maximum = 100%.
[d] T = 540°C.

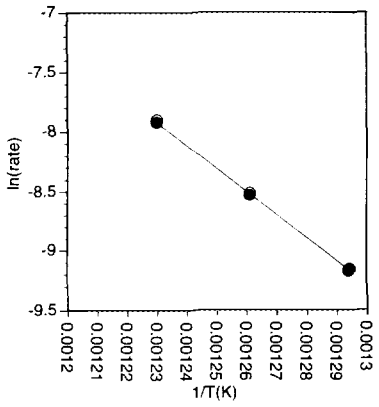

FIG. 2. Arrenhius plot of the 6.4V-AWS and 6.4V-Cab samples.

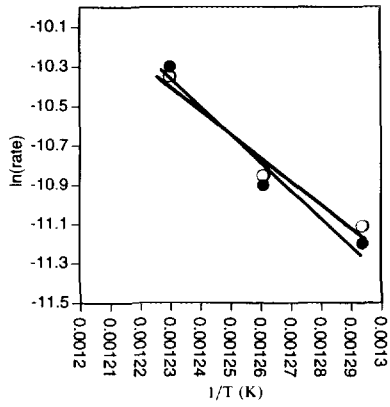

FIG. 3. Arrenhius plot of the 0.58V-AWS (●) and 0.53V-Cab (○) samples.

101 ± 15 kJ/mol for the 0.58V-AWS and 0.53V-Cab samples, respectively, and 164 ± 15 kJ/mol for the 6.4V-AWS and 6.4V-Cab samples. The Arrenhius plots are shown in Figs. 2 and 3. Table 2 shows the rate per mole of vanadium for the AWS samples evaluated at about 5% conversion. The rates were similar on the two samples.

Laser Raman Spectra

The color of the fresh 0.58V-AWS and 0.53V-Cab samples changed from light yellow to white during evacuation to remove adsorbed water, whereas the color of the fresh 6.4V-AWS and 6.4V-Cab samples changed from dark orange to a lighter orange. Figure 4 shows the Raman spectra of the AWS-supported samples. Curve 4D is the spectrum of the fresh 0.58V-AWS sample. The dominant feature in it was the band at 1040 cm^{-1} attributed to a well-dispersed vanadia species (*13–17, 19*) and features of the silica support which are shown in Curve 4F. No peaks indicating the presence of crystalline V_2O_5 (at approximately 998, 703, 526, 480, 404, 304, and 284 cm^{-1} (*25*) as shown in Curve 4A) were observed. The spectrum of the 6.4V-AWS sample is shown in Curve 4B. It showed features characteristic of crystalline V_2O_5 in addition to a peak attributed to the well-dispersed vanadia (1040 cm^{-1}).

Curve 4C shows the Raman spectrum of the 6.4V-AWS samples after reaction. Compared to the spectrum of the fresh sample (Curve 4B), there was a decrease in the intensity of the 1040-cm^{-1} peak relative to the 998-cm^{-1} peak. A 6.4V-AWS sample which had not been exposed to reaction conditions but was treated in a flow of He and O_2 at 520°C and prepared in the same manner as the samples which were treated after reaction did not show any obvious change in the Raman spectrum compared with the fresh sample treated *in vacuo*. Thus, the spectral change was due to use of the samples in reaction and not due to the postreaction treatment.

Figure 5 shows the Raman spectra of the Cabosil silica-supported samples. Curve 5B shows the spectrum of the 6.4V-Cab sample. Similar to the 6.4V-AWS sample (Curve

TABLE 2

Rate per mol V for AWS Supported Samples

T (°C)	Rate (mol/min-mol V) 0.58V-AWS(× 10^2)	Rate (mol/min-mol V) 6.4V-AWS (× 10^2)
500	12.0 ± 0.7	8.3 ± 1.3
520	16.0 ± 1.3	16.0 ± 0.7
540	28.0 ± 3.1	29.0 ± 1.4

Note. Feed: $He/O_2/C_4H_{10}$ = 88/8/4; total flow rate = 100 or 200 cm^3/min; for a conversion of approximately 5.0% butane.

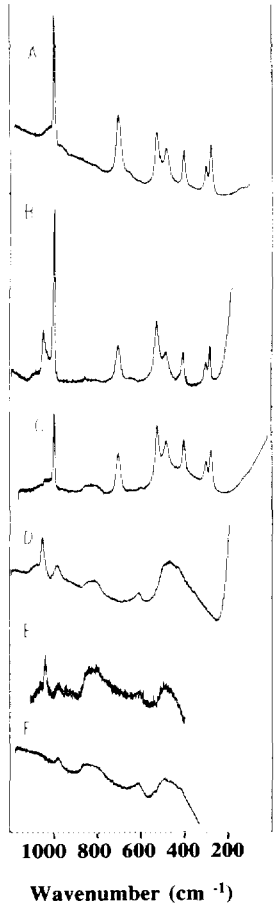

FIG. 4. Laser Raman spectra of (A) unsupported V_2O_5 (untreated), (B) 6.4V-AWS before reaction, (C) 6.4V-AWS after reaction, (D) 0.58V-AWS before reaction, (E) 0.58V-AWS after reaction and (F) AWS. Samples in (B) and (F) were treated *in vacuo* at 520°C for 1 h and exposed to dry O_2 at 520°C for 0.5 h. Spectra were collected in an O_2 atmosphere. Sample (D) was treated *in vacuo* and in dry O_2 as described above at 600°C. Samples in (C) and (E) were exposed to a He/O_2 (10%) feed at 520°C for 3 h after reaction. Spectra were collected in an N_2 atmosphere.

4B), features characteristic of crystalline V_2O_5 were detected as well as the 1040-cm^{-1} peak characteristic of well-dispersed vanadia. However, the ratio of peak areas of dispersed vanadia to crystalline V_2O_5 was much higher for the 6.4V-Cab sample than that for the 6.4V-AWS sample. The spectra of the 0.53V-Cab sample (Curve 5D) was similar to the 0.58V-AWS sample, showing only features characteristic of dispersed vanadia and exposed silica.

Curve 5C shows the Raman spectrum of the 6.4V-Cab sample after reaction. Compared with Curve 5B, a significant decrease in the intensity of the 1040-cm^{-1} peak and

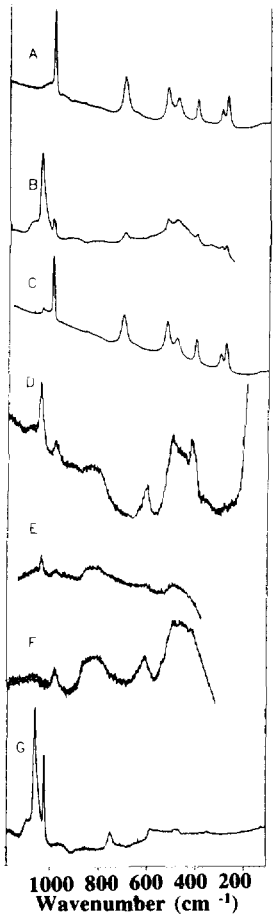

FIG. 5. Laser Raman spectra of (A) unsupported V_2O_5 (untreated), (B) 6.4V-Cab before reaction, (C) 6.4V-Cab after reaction, (D) 0.53V-Cab before reaction, (E) 0.53V-Cab after reaction, (F) Cabosil silica, and (G) 6.4V-Cab treated at 600°C. The sample in (B) was treated *in vacuo* at 520°C for 1 h and exposed to dry O_2 at 520°C for 0.5 h. Spectra were collected in an O_2 atmosphere. Samples (D), (F), and (G) were treated *in vacuo* and in dry O_2 as described above at 600°C. Samples (C) and (E) were exposed to He/O_2 (10%) at 520°C for 3 h after reaction. Spectra were collected in an N_2 atmosphere.

an increase in that of the 998-cm^{-1} peak characteristic of crystalline V_2O_5 were observed. Like the 6.4V-AWS sample, the 6.4V-Cab sample which had not been exposed to reaction conditions but was subjected to the same postreaction treatment showed the same spectrum as that of a fresh sample.

Contrary to the 6.4V-AWS and 6.4V-Cab samples, Curves 4E and 5E show that the spectrum of the 0.58V-AWS and 0.53V-AWS samples after reaction were essentially unchanged compared with the fresh samples.

Curve 5G shows the Raman spectrum of the 6.4V-Cab sample treated *in vacuo* at 600°C but otherwise as described above. It shows a smaller ratio of dispersed vanadia to crystalline V_2O_5 than that on the same sample but treated only to 520°C (Curve 5B). Thus, high-temperature treatment *in vacuo* increased aggregation of the vanadia species.

Thermogravimetric Analysis

The 6.4V-AWS sample was black after reaction before the TGA experiment was conducted. However, the sample regained its original orange color after these experiments. For a 25-mg sample after desorption of water, a consistent weight loss of about 0.2 mg was detected as the temperature was raised from 100 to 600°C. This weight loss was due to carbonaceous deposits on the catalyst burned off by the O_2 in the gas stream minus the weight gain due to oxidation of vanadia. An accurate weight loss beyond the background noise could not be obtained for the 0.58V-AWS sample.

The carbonaceous residue on the used 0.58V-AWS and 6.4V-AWS were detected by treating the samples in O_2 and determining the amounts of CO_2 released. For the experiment with the 0.58V-AWS sample, the amount of CO_2 collected was within error the same as the blank experiment without the catalyst. For the 6.4V-AWS sample, it was 15% higher than that collected in the blank experiment. Thus the color change, the TGA results and these results supported the fact that there was substantially more carbon deposit on the 6.4V-AWS sample than the 0.58V-AWS sample.

TABLE 3

Na and Ca Impurities in Silica

Silica	Na (ppm)	Ca (ppm)
Davison as received	>600	>600
AWS	10	200
Cabosil	0	0

Na and Ca Impurities in Silica

The concentrations of sodium and calcium in the silica samples used as support are shown in Table 3. Acid-washing the Davison silica reduced the levels of Na and Ca to less than 10 and 200 ppm, respectively. Other impurities such as Ti, Al, and Fe were present at levels below 100 ppm. However, acid-washing did not lower the levels of these elements. No Na, Ca, Ti, Al, or Fe were detected in Cabosil silica.

DISCUSSION

Vanadia Structure

The vanadia structure formed on metal oxide-supported samples has been investigated with many different techniques such as X-ray diffraction (*12*), laser Raman spectroscopy (*13–17*), UV–visible spectroscopy (*16*), EXAFS (*26*), ^{51}V NMR (*5, 19, 27*), and ESR (*28*). On silica-supported samples of interest in this study, only two forms of vanadia have been observed: a highly dispersed form of the structure $(Si–O)_3{\equiv}V{=}O$, in which the V ion is in the tetrahedral coordination and the frequency of the stretching vibration of V=O is 1040 cm^{-1}, and crystalline V_2O_5 (*14–17*). The assignment of the 1040 cm^{-1} to a surface species is supported by the fact that this peak is affected reversibly by the hydration–dehydration process (*16, 17*). Due to the weak interaction of vanadia with the

silica support, crystalline V_2O_5 is detected when the vanadia loading is well below a monolayer equivalent. The Raman characterization of the samples in this study (Figs. 4 and 5) shows that these samples are similar to those reported in the literature. Only the 1040-cm^{-1} peak indicating the presence of the $(Si–O)_3{\equiv}V{=}O$ species was evident for the 0.53V-Cab and 0.58V-AWS samples, whereas peaks of both this species and crystalline V_2O_5 were found on the 6.4V-Cab and 6.4V-AWS samples. Since a monolayer equivalent corresponds to loadings of 15 and 29 wt% V, respectively, on AWS and Cabosil silica based on a V-V distance of 0.34 nm as in NH_4VO_3 (*5*), crystalline V_2O_5 are formed at much lower loadings than a monolayer equivalent on these silica supports.

Although it is not trivial without suitable calibration to use intensities of Raman scattered peaks to determine the amounts of dispersed vanadia and crystalline V_2O_5 quantitatively due to the fact that V_2O_5 crystallites are more Raman active than the dispersed species (*10, 11, 15*), one can use them to compare the ratios of these species on different supports. From the relative intensities of the 1040- and 998-cm^{-1} peaks in Curves 4B and 5B, it can be concluded that the ratio of the dispersed vanadia to crystalline V_2O_5 is higher in 6.4V-Cab than in 6.4V-AWS. This may be due to the larger surface area of the Cabosil silica compared to the Davison silica.

The amounts of dispersed vanadia species relative to crystalline V_2O_5 on the two higher loading samples decreased after the samples were used in reaction (Curves 4C and 5C). That is, the dispersed vanadia had aggregated into crystalline V_2O_5 under reaction conditions. On the contrary, only dispersed vanadia was detected on the 0.58-AWS and 0.53V-Cab samples before and after reaction indicating that no detectable aggregation of the well-dispersed vanadia had occurred on these samples.

Aggregation of vanadia into crystalline V_2O_5 was also observed on the high loading silica-supported samples due to thermal treatments. This is evident when Curve 5G for the 6.4V-Cab sample after treatment at 600°C is compared with Curve 5B. However, no aggregation was observed for the lower loading 0.53V-Cab sample after a similar treatment. Treatment at 520°C (the reaction temperature) of the 6.4V-Cab sample either in vacuo or in an He/O_2 flow did not result in any detectable aggregation. Thus, the aggregation observed after use in reaction was not a result of the thermal treatment of the sample. Baiker *et al.* have also observed aggregation of vanadia supported on silica under reaction conditions for the selective catalytic reduction of nitric oxide with ammonia (*29*). They reported that the stability of the well-dispersed vanadia species decreased with increasing reaction temperature and vanadia loading.

Aggregation of vanadia due to reduction has been reported for Al_2O_3- or TiO_2-supported vanadia samples (*30–33*). Thus, the aggregation of vanadia in the SiO_2 samples after reaction in this study might reflect the fact that the vanadia in the high-loading samples is in a reduced state under reaction conditions. This is consistent with the color change of the samples after reaction. The color of the low-loading samples remained light after reaction and their Raman spectra did not change. However, the color of the high loading samples turned dark green or black, which might be a result of reduction of the vanadium ion.

The formation of carbonaceous residues on the surface also contributes to the color change of the sample. The TGA experiments conducted in a He/O_2 atmosphere on the 6.4V-AWS sample after reaction showed a weight loss. The original orange color of the samples was restored after these experiments. In addition, CO_2 was observed to evolve from the sample when heated in O_2. These observations indicate that carbonaceous deposits were formed on the 6.4V-AWS sample during reaction. In contrast, no detectable carbonaceous deposits were formed on the 0.58V-AWS sample,

since they did not turn dark in color after reaction, and no CO_2 evolution was observed when the sample was heated in O_2.

One scenario to explain these data is that the vanadia species undergo redox cycle during reaction, which promotes migration of the dispersed species. In the high-loading samples, the initial concentration of the dispersed vanadia species is high. Thus the probability of agglomeration of these species is also high and crystallites of V_2O_5 are formed readily. The selectivity for dehydrogenation on crystalline V_2O_5 (or V_2O_{5-x}) is much lower than on the dispersed vanadia species. Thus there are more oxygenated surface intermediates produced on the higher loading samples that form carbonaceous deposits.

Reaction Studies

The results of the reaction study shows that the samples differ in two aspects. The selectivity for dehydrogenation is higher (Fig. 1) and the apparent activation energy is lower on the lower loading samples (Figs. 2 and 3). Interestingly, the rate of butane conversion per vanadium is comparable on all samples (Table 2). The differences in dehydrogenation selectivity correlate with the different vanadia structures present under reaction conditions. Catalysts containing well-dispersed vanadia produce higher total dehydrogenation selectivity than the catalysts containing crystalline V_2O_5 (or V_2O_{5-x}).

In the oxidation of butane, the most probable first step involves activating the butane molecule by breaking a C—H bond. Pepera et al. found a deuterium kinetic isotope effect for the oxidation of butane to maleic anhydride over a V—P—O catalyst at the secondary carbon of the butane molecule (*34*). Comparison of the reaction rate of alkanes containing primary, secondary, or tertiary C—H bonds also arrives at a similar conclusion (*35*). After breaking the first C—H bond, a surface alkyl species is formed. Abstraction of the second hydrogen would lead to the production of dehydrogenation products 1-butene, *cis*- or *trans*-2-butene. Further hydrogen abstraction would produce an adsorbed π-allyl species which could lead to the production of 1,3-butadiene (*36*).

Formation of oxygen-containing products such as CO_x and oxygenates involves the insertion of an oxygen atom into the adsorbed species. Whether oxygen is inserted into the adsorbed intermediate and where the insertion occurs are factors which determine the product formed (*37*). If one assumes that lattice oxygen is involved in this oxygen-insertion step, an assumption that has been supported by data in butane oxidation over orthovanadates and vanadia supported on alumina (*38, 39*), then the redox properties of the vanadia should be important in determining the observed selectivity. In particular, the availability, in terms of ease of removal from the lattice, and the number of available lattice oxygen ions at the active site would be the determining factor.

There is no information in this study on the V—O bond involved in the rate-limiting step. It has been suggested in the literature based on indirect observations that the V—O—*M* bridging bond is involved (*35, 40*). This is assumed to apply here also.

The structure of the dispersed vanadia species as proposed in the literature is a vanadyl group bonded to three oxygen ions of the support. Activation of a butane molecule by this species could lead to the formation of species II in Fig. 6. Cleavage of a second C—H bond results in the formation of species III (Fig. 6) which forms species IV after desorption of the alkene. The vanadium in species III is in a reduced state, and it can be reoxidized only by reaction with gaseous oxygen. Thus the active site at this point is inactive for oxidation, and further oxidation of the hydrocarbon species is difficult. On the other hand, reoxidation of a reduced site on the V_2O_{5-x} surface can be rapid due to the high mobility of lattice oxygen at high temperatures (*23*). Thus, a much larger number of oxygen atoms is potentially

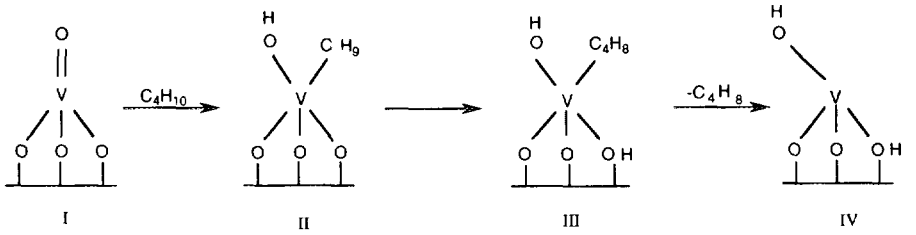

FIG. 6. Schematic of oxidation of butane on dispersed vanadia species.

available for the active sites on crystalline V_2O_5 to oxidize the hydrocarbon species, which causes the catalyst to be less selective.

The above discussion applies to the production of the initial products. As conversion is increased to 10–15%, dehydrogenation selectivity decreases rapidly to less than 10% for the 6.4V-AWS and 6.4V-Cab samples (Fig. 1). The decrease occurs much more rapidly on these than on the lower loading samples. The decrease in dehydrogenation selectivity as the conversion increases is to be expected due to secondary reactions. The difference between the higher and the lower loading samples indicates that secondary reactions occur faster on the former.

It is interesting that lower apparent activation energies (about 110 kJ/mol) are observed for the 0.58V-AWS and 0.53V-Cab samples than the 164 kJ/mol observed for the 6.4V-AWS and 6.4V-Cab samples. If the rate-limiting step is the breaking of the first C–H bond, then the result implies that this step occurs with a lower activation energy on the dispersed vanadia species than on the crystalline V_2O_5 surface. Perhaps this is due to the fact that the vanadium ion in dispersed vanadia (species I, Fig. 6) is tetrahedrally coordinated. This open structure permits the butane molecule a close approach to the V ion. In contrast, the vanadium ion on the (010) plane of V_2O_5 has a square-pyramidal coordination. Thus, the vanadium ion is less accessible to the butane molecule. This results in a higher activation energy for the first reaction step.

In addition to the steric effect, the bridging oxygen proposed to be involved in the first step is bonded to one Si and one V ion in the highly dispersed species, but to two V ions in V_2O_5. The different electronic structures of the oxygen ions could also contribute to the different activation energies.

The trend in activation energy is similar to that for the reduction process. Roozeboom et al. studied the silica-supported vanadia with temperature-programmed reduction (TPR) (*12*). They observed that crystalline V_2O_5 and silica-supported samples which contained crystalline V_2O_5, reduced at higher temperatures than silica-supported samples with dispersed vanadia. Their observation has been reproduced in our laboratory. Since the reduction temperature is related to the magnitude of the activation energy, it can be concluded that the activation energy for reduction by H_2 is lower on the lower loading samples. In this case, the difference in activation energies is most likely due to the different electronic characteristics of the surface bonds involved, since steric effect should be small.

The rates of butane conversion per mol of V are shown in Table 2. They are within a factor of 2 on the two samples. This is interesting considering the differences in dispersion. The 0.58V-AWS and 0.53V-Cab samples contain only dispersed vanadia. It may be assumed that all the vanadium ions are available for reaction. However, the 6.4V-AWS and 6.4V-Cab samples contain small crystallites of vanadium oxide. Thus, only a fraction of the vanadium is on the surface. The data in Table 2 imply that the

vanadia on the surface of the 6.4V-AWS and 6.4V-Cab samples are more active than the dispersed vanadia on the 0.58V-AWS and 0.53V-Cab samples. The difference, however, should be less than a factor of ten because the crystallites of V_2O_5 are so small that they are not detectable by ordinary X-ray diffraction.

The similarity in the reaction rates on the different samples is interesting in view of the different activation energies. It suggests a compensation effect, that is, the preexponential factor is smaller for the lower loading samples. A smaller preexponential factor could be interpreted as a more negative entropy of activation ($\Delta S\ddagger$), that is, the transition state is more rigidly bound. This is consistent with the picture presented earlier that on the lower loading sample, the butane molecule can have a closer approach to the dispersed vanadia site. This closer approach leads to a lower activation energy, while tighter bonding and stronger interaction produces a more negative $\Delta S\ddagger$. To account for the data by this effect alone, $\Delta S\ddagger$ needs to be more negative by at least 37 J/K-mol for the lower loading sample, which is close to the value of one degree of freedom of the translational motion.

The above discussion assumes that the same rate-limiting step of C—H bond breaking applies to both high- and low-loading samples. However, the possibility that the vanadia species in the high loading samples are in a reduced state under reaction conditions, whereas those in the low loading samples are in the fully oxidized state would suggest that the rate-limiting steps are different on the different samples. To be in a reduced state, the rate of reoxidation by gaseous oxygen of the high loading samples must be relatively slow compared to the other steps in the reaction sequence. If so, the different activation energies for samples of different loadings would be the result of different rate-limiting steps.

CONCLUSION

The catalytic properties in the oxidation of butane and the structure of vanadia species on silica-supported catalysts were found to depend on the loading. Only highly dispersed vanadia existed on the 0.56V-AWS and 0.53V-Cab samples, while crystalline V_2O_5 species as well as dispersed vanadia existed on the 6.4V-AWS and 6.4V-Cab samples. The vanadia on the 6.4V-AWS and 6.4V-Cab samples had low stability and tended to aggregate under reaction conditions and at elevated temperatures. The highly dispersed species in the 0.56V-AWS and 0.53V-Cab samples remained unchanged under reaction conditions and at elevated temperatures. These latter samples were more selective to dehydrogenation products in butane oxidation and exhibited lower activation energies for the reaction. The differences in selectivity were attributed to the availability of lattice oxygen atoms (in terms of number) being higher on the samples containing crystalline V_2O_5 than those with dispersed vanadia. The difference in the activation energy was due either to the different steric effects in the approach of a butane molecule to the active sites or to different rate-limiting steps.

ACKNOWLEDGMENTS

This work was supported by the U.S. Department of Energy, Division of Basic Energy Sciences. Lynne Owens also acknowledged the 3M Company for a fellowship and the Monsanto Company for the minority faculty internship.

REFERENCES

1. Wainwright, M. S., and Foster, N. R., *Catal. Rev.-Sci. Eng.* **19**(2), 211 (1979).
2. Nikolov, V., Klissurski, D., and Anastasov, A., *Catal. Rev.-Sci. Eng.* **33**(3), 319 (1991).
3. Went, G. T., Leu, L., and Bell, A. T., *J. Catal.* **134,** 479 (1992).
4. Kozlowski, R., Pettifer, R. F., and Thomas, J. M., *J. Phys. Chem.* **87,** 5176 (1983).
5. Eckert, H., and Wachs, I. E., *J. Phys. Chem.* **93,** 6796 (1989).
6. Vorobev, L. N., Badalova, I. K., and Razikov, K. Kh., *Kinet. Katal.* **23,** 119 (1982).
7. Richter, M., Heise, K., and Öhlmann, G., *React. Kinet. Catal. Lett.* **27,** 109 (1985).
8. Kijenski, J., Baiker, A., Glinski, M., Dollenmeier, P., and Wokaun, A., *J. Catal.* **101,** 1 (1986).

9. Haber, J., Kozlowska, A., and Kozlowski, R., *J. Catal.* **102,** 52 (1986).
10. Roozeboom, F., Fransen, T., Mars, P., and Gellings, P. J., *Z. Anorg. Allg. Chem.* **449,** 25 (1979).
11. Roozeboom, F., Medema, J., and Gellings, P. J., *Z. Phys. Chem.* **111,** 215 (1978).
12. Roozeboom, F., Mittelmeijer-Hazeleger, M. C., Moulijn, J. A., Medema, J., de Beer, V. H. J., and Gellings, P. J., *J. Phys. Chem.* **84,** 2783 (1980).
13. Deo, G. and Wachs, I. E., *J. Phys. Chem.* **95,** 5889 (1991).
14. Oyama, S. T., Went, G. T., Lewis, K. B., Bell, A. T., and Somorjai, G. A., *J. Phys. Chem.* **93,** 6786 (1989).
15. Miyata, H., Tokuda, S., and Yoshida, T., *Appl. Spectrosc.* **43,** 522 (1989).
16. Schraml-Marth, M., Wokaun, A., Pohl, M., and Krauss, H. L., *J. Chem. Soc. Faraday Trans.* **87,** 2635 (1991).
17. Went, G. T., Oyama, S. T., and Bell, A. T., *J. Phys. Chem.* **94,** 4240 (1990).
18. Oyama, S. T., *Res. Chem. Int.* **15,** 165 (1991).
19. Le Coustumer, L. R., Tauok, B., Le Meur, M., Payen, E., Guelton, M., and Grimblot, J., *J. Phys. Chem.* **92,** 1230 (1988).
20. Erdohelyi, A., and Solymosi, F., *Appl. Catal.* **39,** L11 (1988).
21. Erdohelyi, A., and Solymosi, F., *J. Catal.* **123,** 31 (1990).
22. Erdohelyi, A., and Solymosi, F., *J. Catal.* **129,** 497 (1991).
23. Oyama, S. T., and Somorjai, G. A., *J. Phys. Chem.* **94,** 5022 (1990).
24. Le Bars, J., Auroux, A., and Vedrine, J. C., *Stud. Surf. Sci. Catal.* **72,** 181 (1992).
25. Abello, L., Husson, E., Repelin, Y., and Lucazeau, G., *Spectrochim. Acta Part A* **39,** 641 (1983).
26. Tanaka, T., Yamashita, H., Tsuchitani, R., Funabiki, T., and Yoshida, S., *J. Chem. Soc. Faraday Trans 1* **84**(9), 2987 (1988).
27. Eckert, H., and Wachs, I. E., *Mater. Res. Soc. Symp. Proc.* **111,** 459 (1988).
28. Sharma, V. K., Wokaun, A., and Baiker, A., *J. Phys. Chem.* **90,** 2715 (1986).
29. Baiker, A., Dollenmeier, P., Glinski, M., Reller, A., and Sharma, V. K., *J. Catal.* **111,** 273 (1988).
30. Andersen, P. J., and Kung, H. H., *J. Phys. Chem.* **96,** 3114 (1992).
31. Sobalik, Z., Kozlowski, R., and Haber, J., *J. Catal.* **127,** 665 (1991).
32. Odriozola, J. A., Soria, J., Somorjai, G. A., Heinemann, H., Gracia de la Banda, J. F., Lopez Granados, M., and Conesa, J. C., *J. Phys. Chem.* **95,** 240 (1991).
33. Topsøe, N., *J. Catal.* **128,** 499 (1991).
34. Pepera, M. A., Callahan, J. L., Desmond, M. J., Milberger, E. C., Blum, P. R., and Bremer, N. J., *J. Am. Chem. Soc.* **107,** 4883 (1985).
35. Patel, D., Kung, M. C., and Kung, H. H., *in* "Proceedings, 9th International Congress on Catalysis, Calgary, 1988" (M. J. Phillips and M. Ternan, Eds.), Vol. 4, p. 1554. Chem. Inst. of Canada, Ottawa, 1988.
36. Kung, H. H., *Ind. Eng. Chem. Prod. Res. Dev.* **25,** 171 (1986).
37. Kung, H. H., Michalakos, P. M., Owens, L., Kung, M. C., Andersen, P. J., Owen, O. S., and Jahan, I., "ACS Symp. Ser. 523, Catalytic Selective Oxidation," (S. T. Oyama, and J. W. Hightower, Eds.), 1993, p. 389.
38. Andersen, P. J., and Kung, H. H., Proc. 10th Intern. Congr. Catal., (L. Guczi, F. Solymosi, and P. Teteryi, Eds.), Akademiai Kiado Publ., Budapest, 1993, p. 205.
39. Owen, O. S., Kung, M. C., and Kung, H. H., *Catal. Lett.* **12,** 45 (1992).
40. Deo, G. and Wachs, I. E., *J. Catal.* **129,** 307 (1991).